Electronic Supplementary Information (ESI)

Nanoporous PtCuTi alloy with low Pt content and greatly enhanced electrocatalytic performance towards methanol oxidation and oxygen reduction

Ying Wang,[a] Kuibo Yin,[b] Jie Zhang,[a] Conghui Si,[a] Xiaoting Chen,[a] Lanfen Lv,[a] Wensheng Ma,[a] Hui Gao,[a] Zhonghua Zhang[a, *]

[a]Key Laboratory for Liquid-Solid Structural Evolution and Processing of Materials (Ministry of Education), School of Materials Science and Engineering, Shandong University, Jingshi Road 17923, Jinan, 250061, P.R. China

[b]SEU-FEI Nano-Pico Center, Key Lab of MEMS of Ministry of Education, Southeast University, Nanjing 210096, P.R. China

[*]Corresponding author. Email: zh_zhang@sdu.edu.cn, TEL/FAX: +86-531-88396978

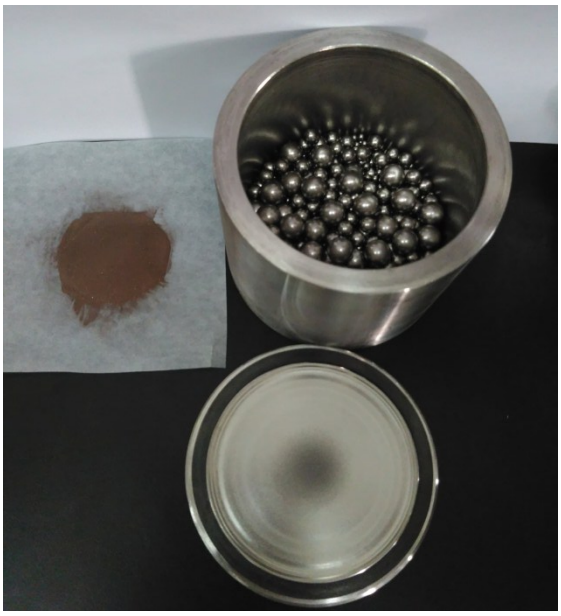

Figure S1. Photograph of the mechanically alloyed $Cu_{92}Ti_5Pt_3$ powders (left) and a set of the milling tank with balls (right). For each milling tank, about 25 g alloy powders could be prepared after mechanical alloying. For the planetary ball mill machine with four sets of the milling tanks, the precursor powders of up to 100 g can be produced after one batch of mechanical alloying.

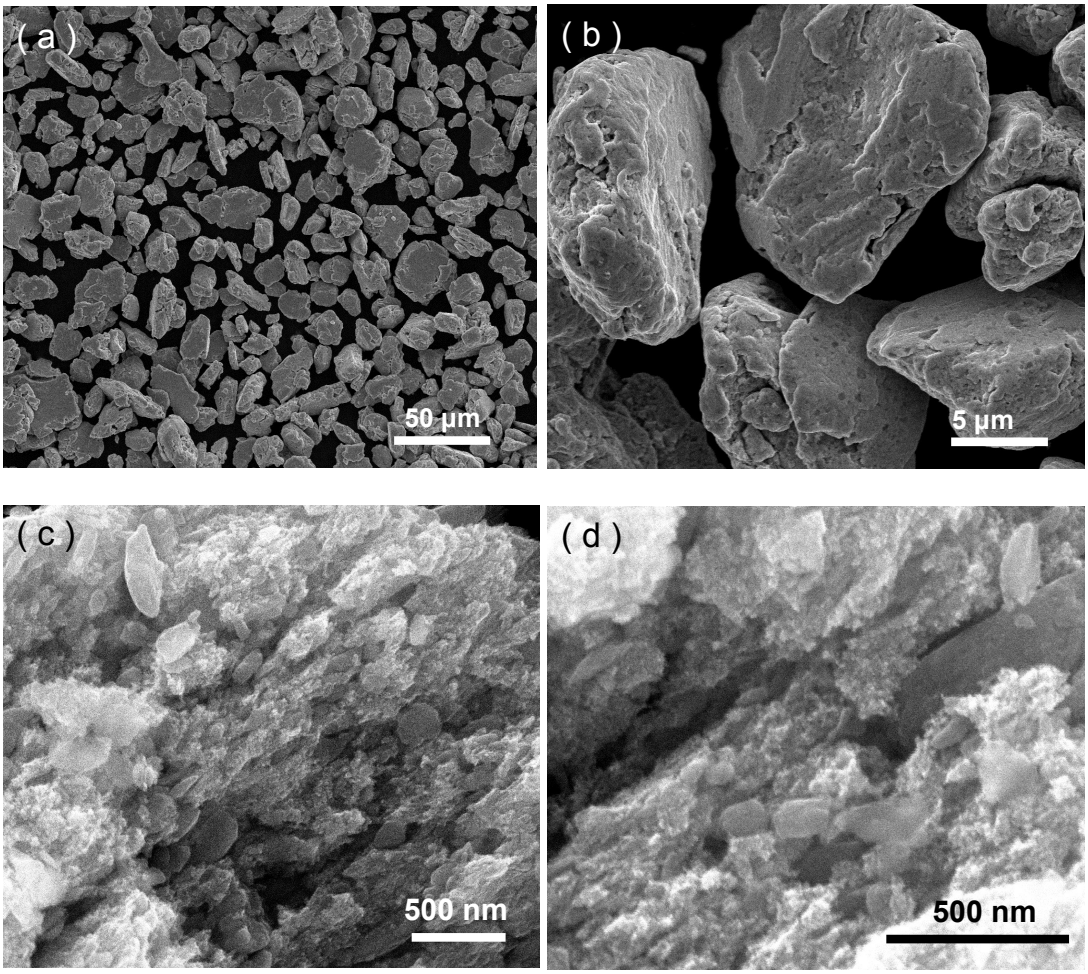

Figure S2. SEM images showing the microstructure of (a, b) the mechanically alloyed $Cu_{92}Ti_5Pt_3$ powders and (c, d) the as-dealloyed np-PtCuTi samples.

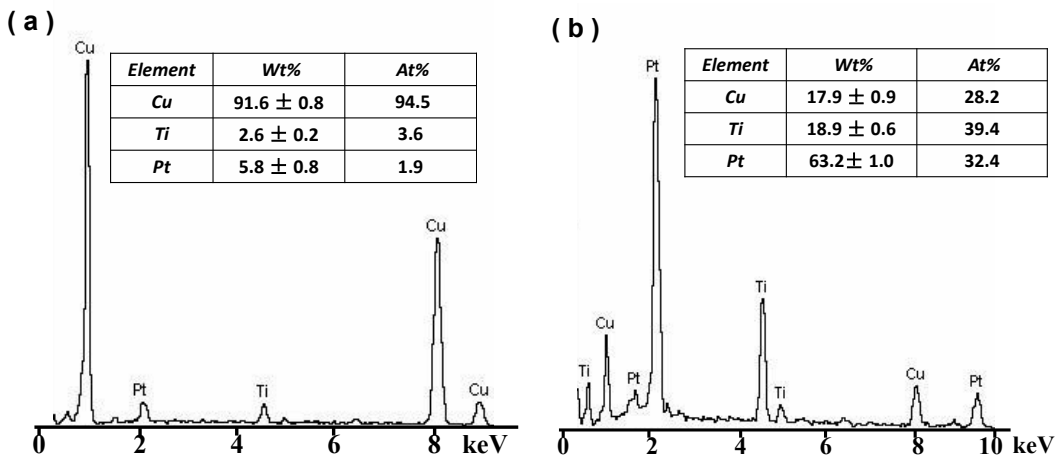

Element	Wt%	At%
Cu	91.6 ± 0.8	94.5
Ti	2.6 ± 0.2	3.6
Pt	5.8 ± 0.8	1.9

Element	Wt%	At%
Cu	17.9 ± 0.9	28.2
Ti	18.9 ± 0.6	39.4
Pt	63.2± 1.0	32.4

Figure S3. Typical EDX spectra and corresponding elemental contents of (a) the as-milled $Cu_{92}Ti_5Pt_3$ precursor powders and (b) the as-dealloyed np-PtCuTi alloy.

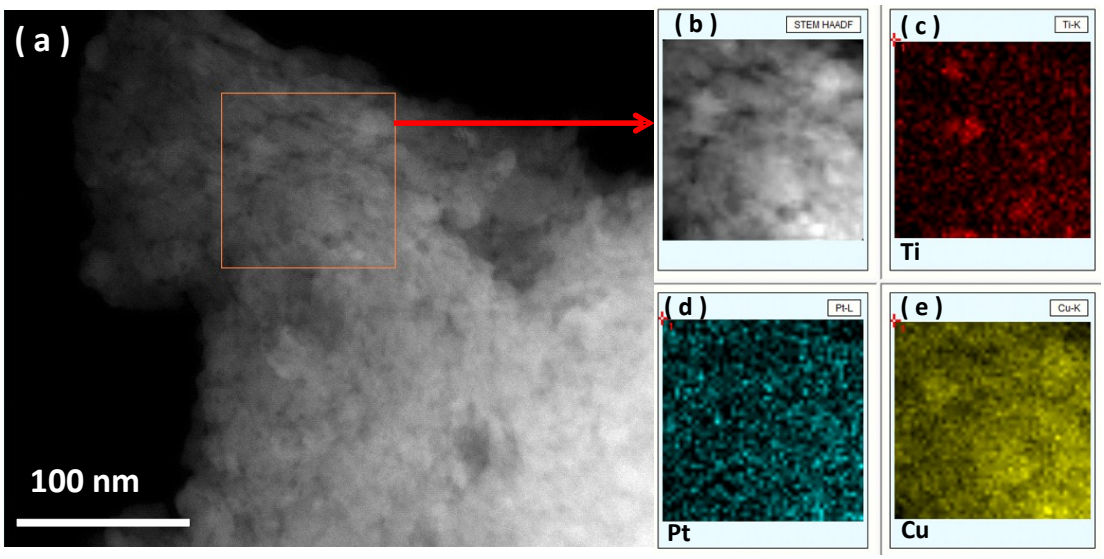

Figure S4. (a) STEM image showing the microstructure of the mechanically alloyed $Cu_{92}Ti_5Pt_3$ sample. (b) The marked area for EDX-mapping (100 nm × 100 nm). (c-e) EDX mapping images corresponding to the marked area in (a).

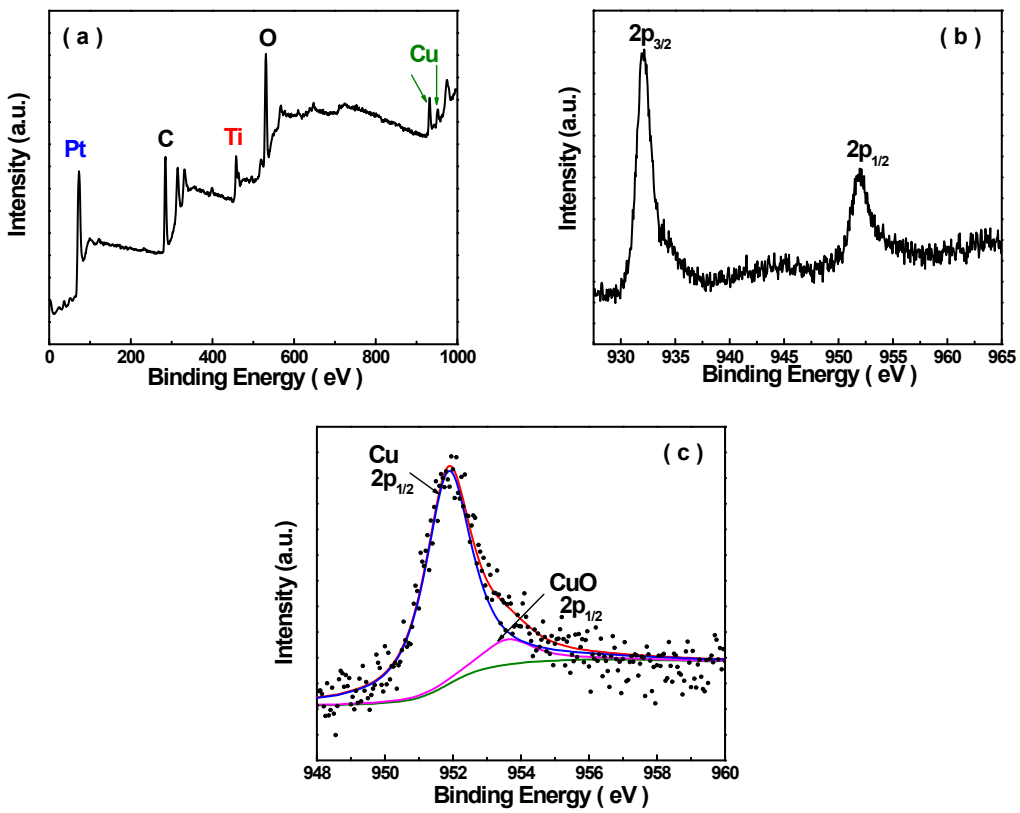

Figure S5. (a) XPS broad scan spectrum of the np-PtCuTi alloy. XPS spectra of (b) Cu 2p and (c) Cu $2p_{1/2}$ for the np-PtCuTi alloy.

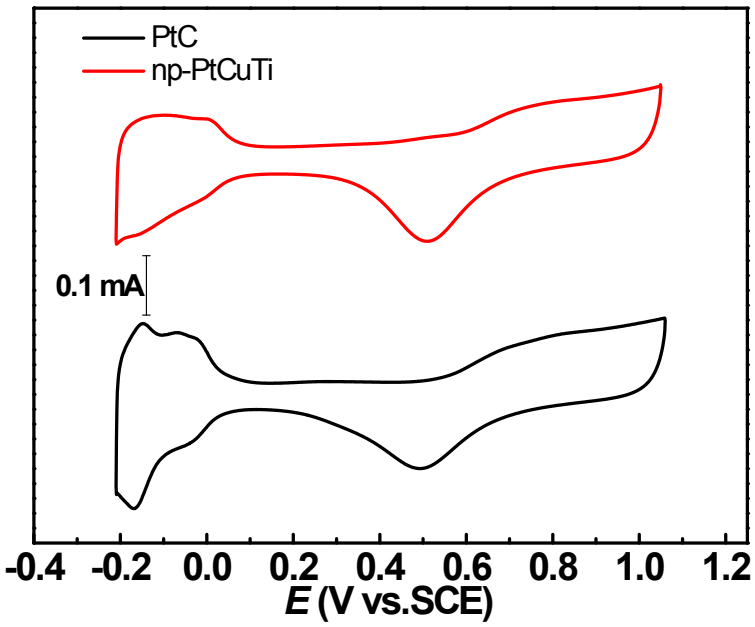

Figure S6. Stable CVs of the np-PtCuTi and PtC catalysts in the N_2-purged 0.5 M H_2SO_4 solution. (Scan rate: 50 mV s^{-1})

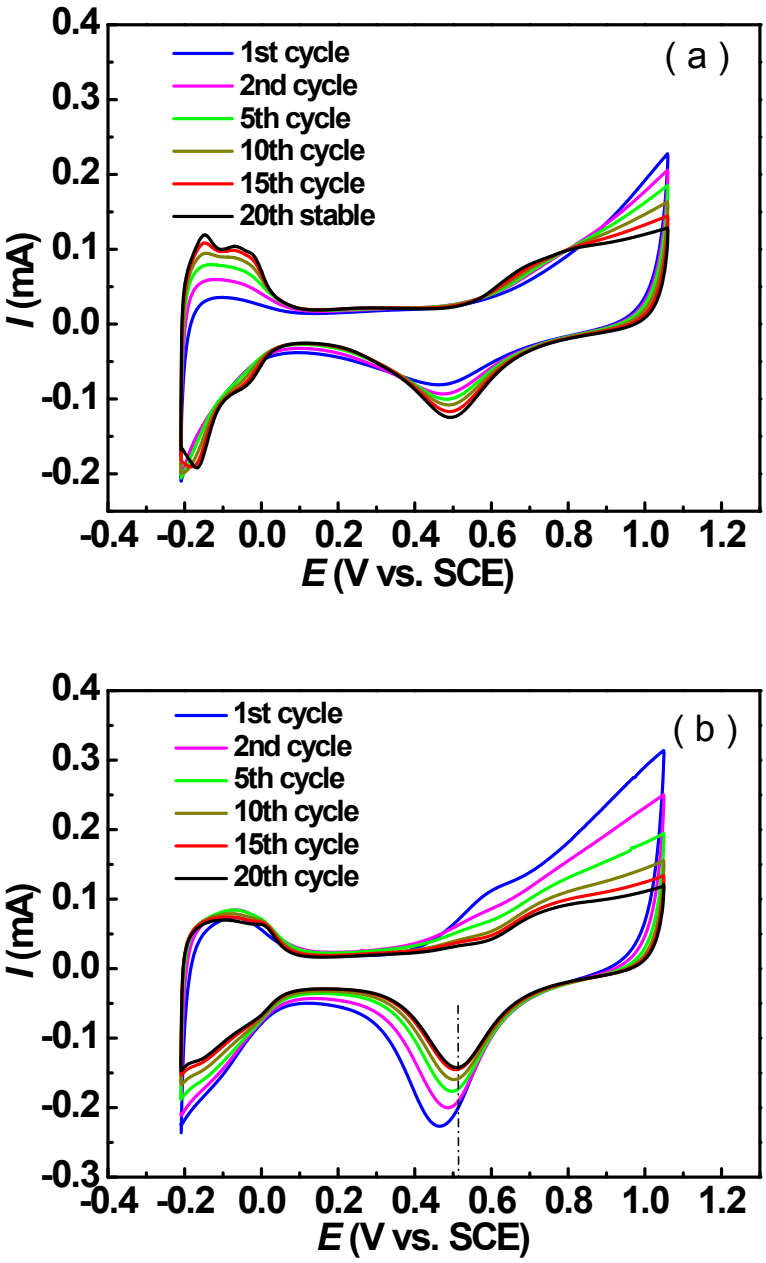

Figure S7. The evolution of CV curves of (a) PtC and (b) the np-PtCuTi alloy in the N_2-purged 0.5 M H_2SO_4 solution. (Scan rate: 50 mV s^{-1})

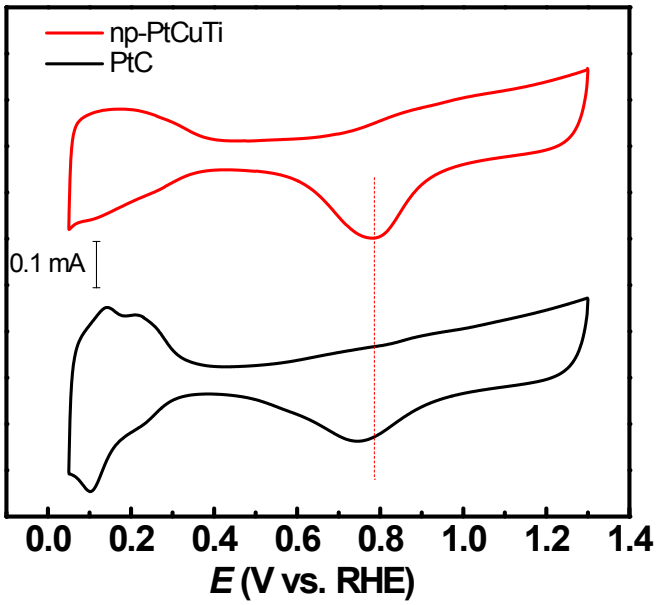

Figure S8. Stable CV curves of the np-PtCuTi and PtC catalysts in the N_2-purged 0.1 M $HClO_4$ solution. (Scan rate: 50 mV s^{-1})

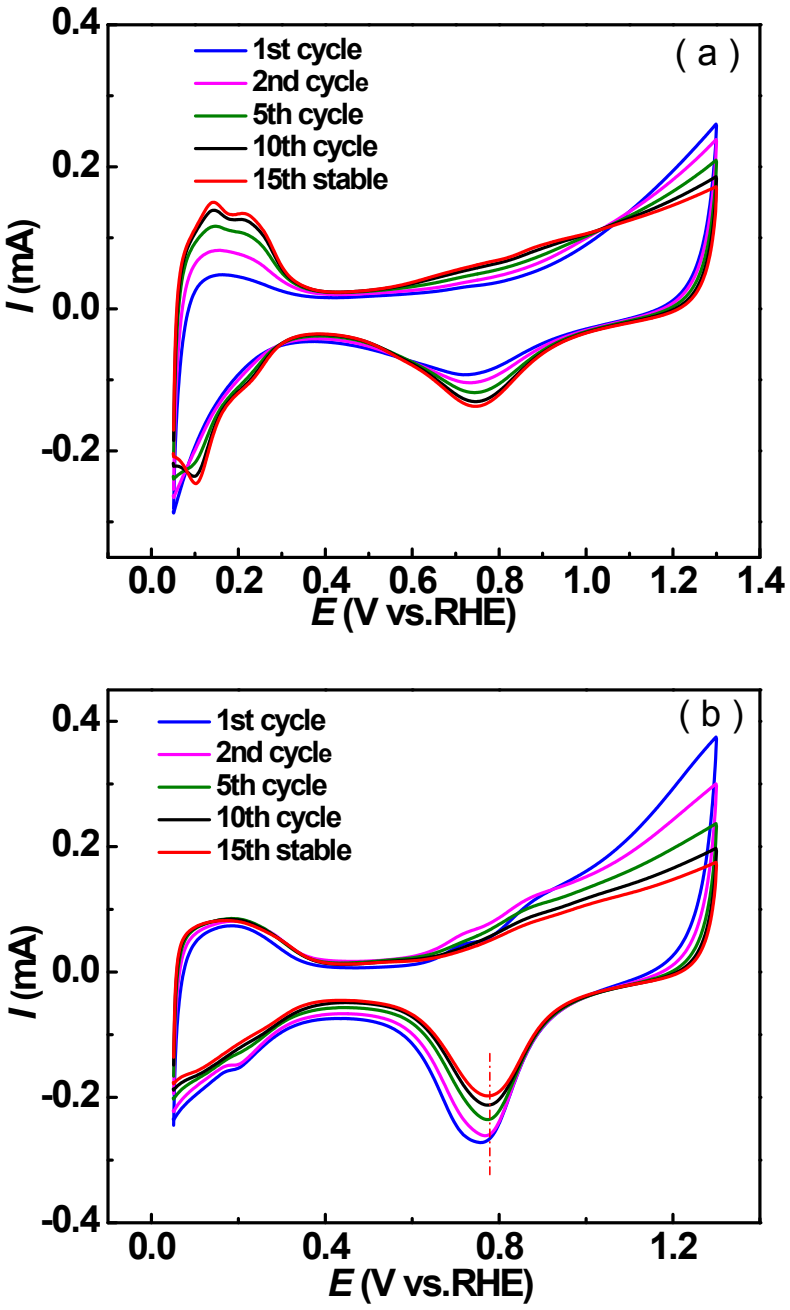

Figure S9. The evolution of CV curves of (a) PtC and (b) the np-PtCuTi alloy in the N_2-purged 0.1 M $HClO_4$ solution. (Scan rate: 50 mV s^{-1})

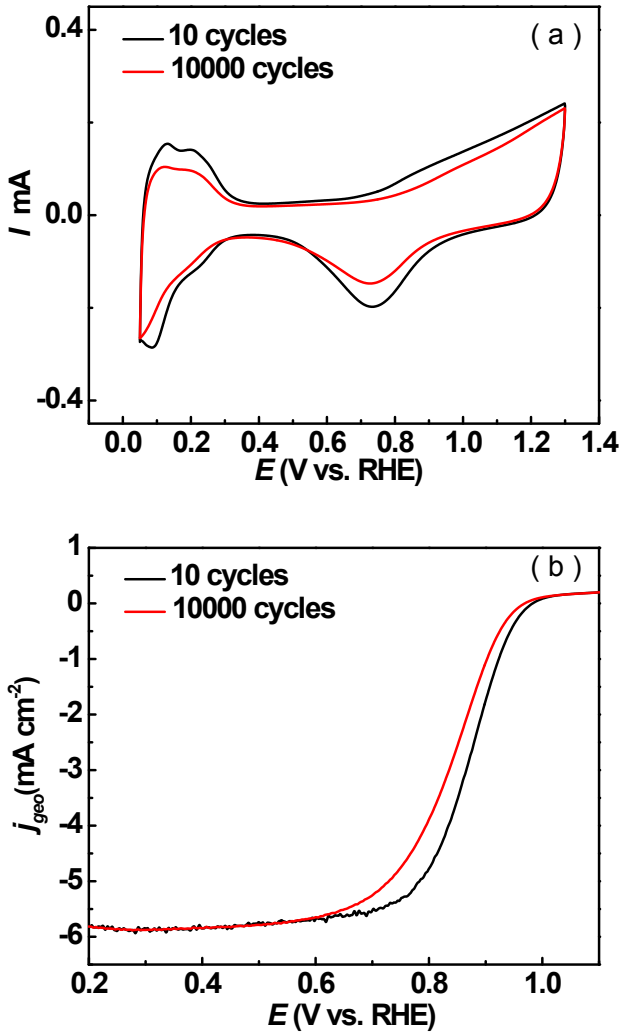

Figure S10. (a) CVs and (b) ORR polarization curves for the PtC catalyst after 10 and 10000 potential cycles in the O_2-saturated 0.1 M $HClO_4$ solution.

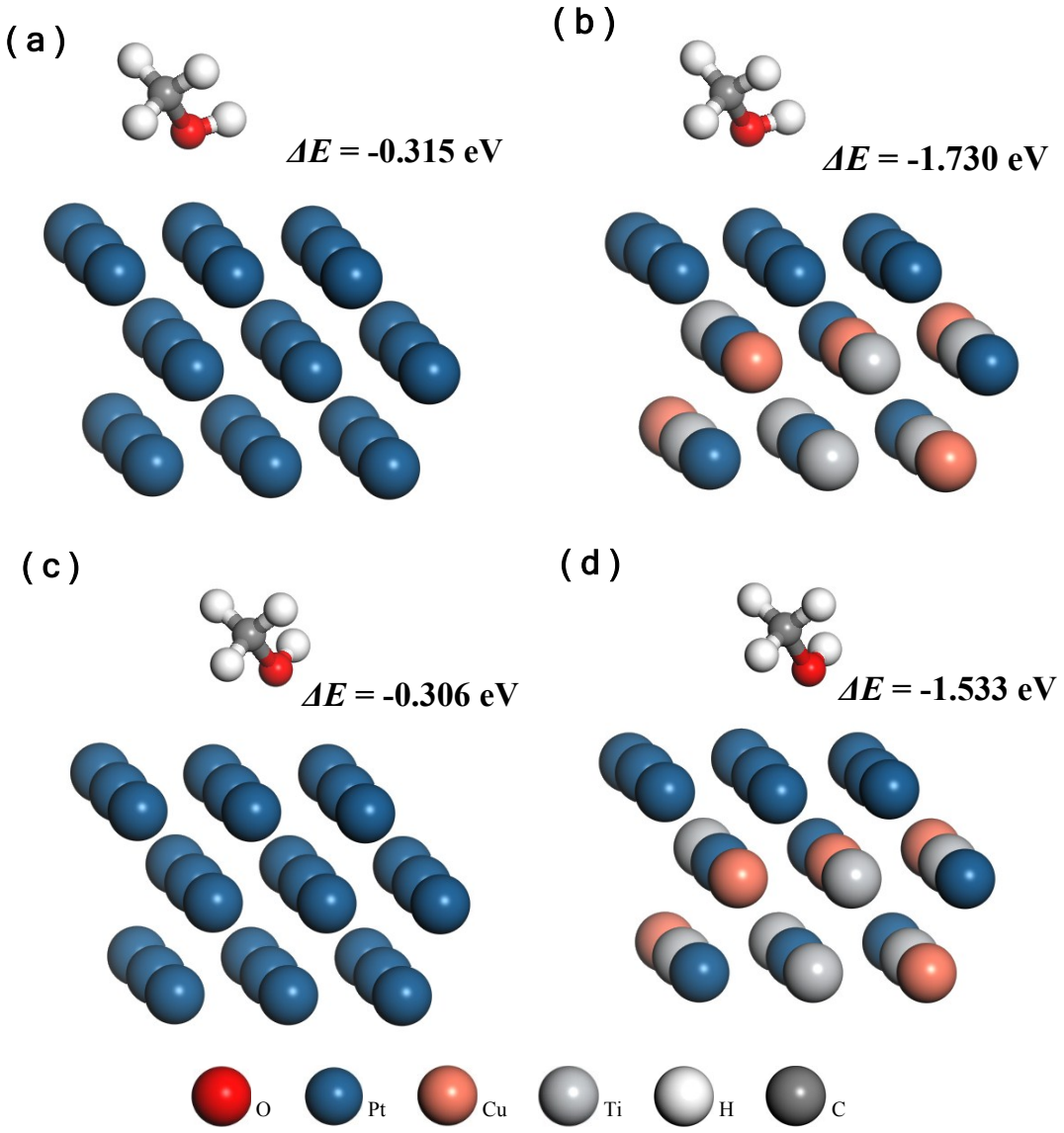

Figure. S11. The schematic model of methanol adsorbed on Pt (111) and PtCuTi (111) slabs: (a,b) top site, (c,d) bridge site.

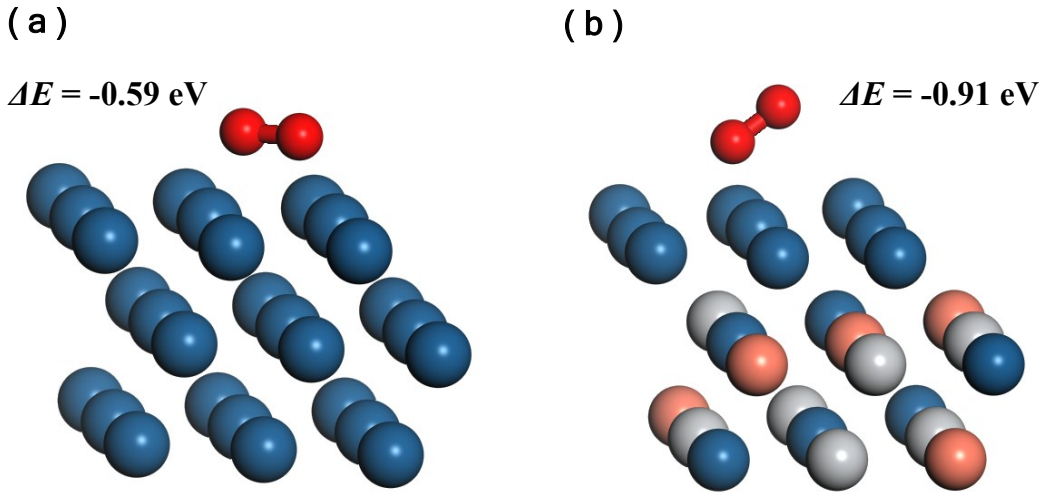

Figure. S12. The schematic model of oxygen adsorbed on (a) the bridge site of Pt (111) and (b) the top site of PtCuTi (111).

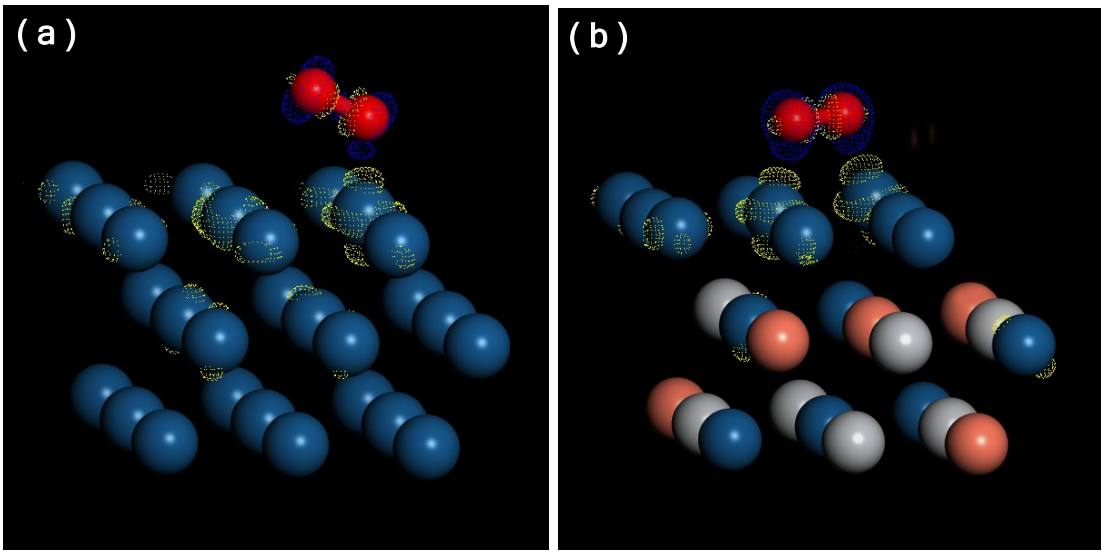

Figure. S13. Difference electron density maps highlighting the electron charge density redistribution due to the O_2 adsorption on the (a) Pt (111) and (b) PtCuTi (111) surfaces. Yellow and blue colors represent depletion and accumulation of electrons, respectively.

Table S1. Comparison of MOR parameters for the np-PtCuTi alloy and commercial PtC catalyst for methanol electro-oxidation in the 0.5 M H_2SO_4 and 0.5 M H_2SO_4 + 0.5 M CH_3OH solution.

Sample	MOR						CO
	E_{onset} (V) (vs. SCE)	E_{peak} (V) (vs. SCE)	j_{ECSA} (mA cm^{-2})	j_{mass} (mA mg$^{-1}_{Pt}$)	I_f/I_b	ECSA (m^2 g^{-1})	E_{peak} (V) (vs. SCE)
PtC	0.14	0.62	0.5	230	0.85	46	0.67
np-PtCuTi	0.17	0.61	2.5	721	1.36	29	0.51
RSD of np-PtCuTi	1.9%	0.8%	7.3%	3.9%	7.6%	4.8%	2.9%

Abbreviations: RSD, relative standard deviation

Table S2. Comparison of the MOR activity of our np-PtCuTi alloy with that of previously reported state-of-the-art electrocatalysts.

Sample	*ref*	MOR			
		j_{ECSA} (mA cm^{-2})	IF of SA (vs PtC)	j_{mass} (mA mg$^{-1}_{Pt}$)	IF of MA (vs PtC)
Our np-PtCuTi	--	**2.50**	**5**	**721**	**3.1**
Np-$Pt_{60}Cu_{40}$	1	4.90	4.9	750	--
Np-PtCu	2	4.00	4	730	1.6
Spiny-porous Pt nanotubes	3	0.55	3.2	260	1.5
Tetrahexahedral Pt−Ni nanoframes	4	2.19	2.63	840	3.9
Hollow Pt_4Ru	5	0.62	2.5	--	--
Dendritic Pt–Ni–P alloy nanoparticles	6	0.65	2.3	360	2.4
Nanoporous Pd_{27}@Pt_{73} particles	7	--	--	490	2.1
TeCuPt nanowires	8	--	--	245	2.3
Pt–MoO_3–RGO hollow nanorods	9	--	--	~770	~1.9
PtFe@Pt nanodendrites	10	--	--	821	2.5

Abbreviations: SA, specific activity; MA, mass activity; IF, improvement factor.

Table S3. Comparison of ORR parameters for the np-PtCuTi alloy and commercial PtC catalyst for ORR in the 0.1 M $HClO_4$ solution.

Sample	ORR			
	E_{half} (V) (vs. RHE)	$j_{ECSA,0.90V}$ (mA cm^{-2})	$j_{mass,0.90V}$ (mA mg^{-1}_{Pt})	ECSA (m^2 g^{-1})
PtC	0.864	0.20	135	66
np-PtCuTi	0.908	0.84	256	30.5
RSD of np-PtCuTi	0.3%	6.9%	8.3%	4.8%

Abbreviations: RSD, relative standard deviation

Table S4. Comparison of ORR parameters for the np-PtCuTi alloy after different cycling numbers in the oxygen-saturated 0.1 M $HClO_4$ solution.

Cycling number	E_{half} (V) (vs. RHE)	ORR		
		$j_{ECSA,0.90V}$ (mA cm^{-2})	$j_{mass,0.90V}$ (mA mg^{-1}_{Pt})	ECSA (m^2 g^{-1})
10	0.908	0.84	256	30.5
5000	0.903	0.92	239	25.9
10000	0.901	0.88	225	25.5
15000	0.903	1.05	233	21.85
20000	0.903	1.10	234	20.89

Table S5. Comparison of the ORR activity of our np-PtCuTi alloy with the state-of-the-art ORR electrocatalysts from the previous literatures.

materials	*ref*	ORR		
		$j_{ECSA,0.90V}$ (mA cm^{-2})	$j_{mass,0.90V}$ (mA mg$^{-1}_{Pt}$)	E_{half} (V vs. RHE)
Porous hollow $PtNi_3$/C	11	1.29	564	--
Octahedral PtNiIr nanoparticle	12	1.03	511	0.912
our np-PtCuTi	--	**0.84**	**256**	**0.908**
Pt–Fe nanodendrites	13	0.82	~240	--
Np-PtRuCuOsIr	14	0.77	249	0.900
$Pt_{78}Cu_{22}$ nanodendrites	15	0.63	320	--
Np-Pt_3Cu	16	0.61	189	0.905
Pt/V-TiO2	17	0.57	--	0.873
Pt/$Ti_{0.9}Co_{0.1}N$	18	0.54	460	0.905
Np-PtTi	19	0.52	320	--
Np-PtPdAlCu	20	0.50	177	0.880
PtPd nanocage–rGO	21	0.48	534	0.953
Cu−Pt Nanocage	22	0.47	320	0.846
Pd_9Ru@Pt/C	23	0.26	380	--
Pt/GC–Fe_2MoC	24	--	267.7	--

Table S6. Comparison of the ORR durability of our np-PtCuTi alloy with those of the previously reported state-of-the-art ORR electrocatalysts.

	ORR durability						
material	cycling number	voltage range (vs. RHE)	RR of SA	RR of MA	ΔE_{half} (mV)	RR of ECSA	*ref*
Octahedra PtNiCo/C	6000	0.6- 1.1 V	--	37.6%	24	--	25
PtPd nanocage–rGO	10000	0.6-1.05 V	73.6%	71%	9	88.7%	21
Octahedral Pt−Ni	4000	0.6-1.0 V	54.4%	48.5%	~20	92%	26
$Au_{1.03}Pt$/C decahedra	30000	0.6-1.0 V	~90%	~80%	17	--	27
PtNi octahedra	10000	0.6-1.1 V	108%	93%	~0	89%	28
Octahedral Pt_2CuNi	4000	0.6-1.0 V	78%	81.3%	~10	95.6%	29
Octahedral PtNiIr nanoparticle	10000	0.6-1.0 V	73%	66%	--	--	12
Np-PtRuCuOsIr	15000	0.6-1.0 V	73.1%	50%	25	63.1%	14
$Pt_{78}Cu_{22}$ nanodendrites	5000	0.6-1.1 V	--	--	23	88%	15
our np-PtCuTi	**20000**	**0.6-1.0 V**	**130%**	**91%**	**5**	**68.5%**	--

Abbreviations: RR, retention rate.

References

1. H. J. Qiu, X. Shen, J. Q. Wang, A. Hirata, T. Fujita, Y. Wang and M. W. Chen, *Acs Catal.,* 2015, **5**, 3779-3785.
2. H. J. Qiu, H. T. Xu, X. Li, J. Q. Wang and Y. Wang, *J. Mater. Chem. A*, 2015, **3**, 7939-7944.
3. Y. Zuo, K. Cai, L. Wu, T. Li, Z. Lv, J. Liu, K. Shao and H. Han, *J. Mater. Chem. A*, 2015, **3**, 1388-1391.
4. J. Ding, L. Bu, S. Guo, Z. Zhao, E. Zhu, Y. Huang and X. Huang, *Nano lett.*, 2016, **16**, 2762-2767.
5. Y. Hu, A. Zhu, Q. Zhang and Q. Liu, *J. Power Sources*, 2015, **299**, 443-450.
6. J. Zhang, K. Li and B. Zhang, *Chem. Commun.*, 2015, **51**, 12012-12015.
7. B. Jiang, C. Li, J. Henzie, T. Takei, Y. Bando and Y. Yamauchi, *J. Mater. Chem. A*, 2016, **4**, 6465-6471.
8. H. Li, C. Ren, S. Xu, L. Wang, Q. Yue, R. Li, Y. Zhang, Q. Xue and J. Liu, *J. Mater. Chem. A*, 2015, **3**, 5850-5858.
9. L. Wang, L. Liang, F.Lu, X. Tong and R. Li, *J. Mater. Chem. A*, 2016, 4, 1923-1930.
10. J. Zhu, M. Xiao, K. Li, C. Liu and W. Xing, *Chem. Commun.*, 2015, **51**, 3215-3218.
11. L. Dubau, T. Asset, R. Chattot, C. Bonnaud, V. Vanpeene, J. Nelayah and F. Maillard, *ACS Catal.*, 2015, **5**, 5333-5341.

12. T. Yang, G. Cao, Q. Huang, Y. Ma, S. Wan, H. Zhao, N. Li, F. Yin, X. Sun, D. Zhang and M. Wang, *J. Power Sources*, 2015, **291**, 201-208.

13. J. Mao, Y. Chen, J. Pei, D. Wang and Y. Li, *Chem. Commun.*, 2016, **52**, 5985-5988.

14. X. Chen, C. Si, Y. Gao, J. Frenzel, J. Sun, G. Eggeler and Z. Zhang, *J. Power Sources*, 2015, **273**, 324-332.

15. S. Fu, C. Zhu, Q. Shi, H. Xia, D. Du and Y. Lin, *Nanoscale*, 2016, **8**, 5076-5081.

16. J. Sun, J. Shi, J. Xu, X. Chen, Z. Zhang and Z. Peng, *J. Power Sources*, 2015, **279**, 334-344.

17. J.-H. Kim, G. Kwon, H. Lim, C. Zhu, H. You and Y.-T. Kim, *J. Power Sources*, 2016, **320**, 188-195.

18. Y. Xiao, G. Zhan, Z. Fu, Z. Pan, C. Xiao, S. Wu, C. Chen, G. Hu and Z. Wei, *J. Power Sources*, 2015, **284**, 296-304.

19. H. Duan, Q. Hao and C. Xu, *J. Power Sources*, 2015, **280**, 483-490.

20. X. Chen, Y. Jiang, J. Sun, C. Jin and Z. Zhang, *J. Power Sources*, 2014, **267**, 212-218.

21. S. Bai, C. Wang, W. Jiang, N. Du, J. Li, J. Du, R. Long, Z. Li and Y. Xiong, *Nano Res.*, 2015, **8**, 2789-2799.

22. V. M. Dhavale and S. Kurungot, *ACS Catal.*, 2015, **5**, 1445-1452.

23. Y. Sun, Y.-C. Hsieh, L.-C. Chang, P.-W. Wu and J.-F. Lee, *J. Power Sources*, 2015, **277**, 116-123.

24. Z. Yan, M. Zhang, J. Xie and P. K. Shen, *J. Power Sources*, 2015, **295**, 156-161.

25. X. Huang, Z. Zhao, Y. Chen, E. Zhu, M. Li, X. Duan and Y. Huang, *Energy Environ. Sci.*, 2014, **7**, 2957-2962.

26. C. Zhang, S. Y. Hwang, A. Trout and Z. Peng, *J. Am. Chem. Soc.*, 2014, **136**, 7805-7808.

27. T. Bian, H. Zhang, Y. Jiang, C. Jin, J. Wu, H. Yang and D. Yang, *Nano lett.*, 2015, **15**, 7808-7815.

28. E. Zhu, Y. Li, C.-Y. Chiu, X. Huang, M. Li, Z. Zhao, Y. Liu, X. Duan and Y. Huang, *Nano Res.*, 2015, **9**, 149-157.

29. C. Zhang, W. Sandorf and Z. Peng, *ACS Catal.*, 2015, **5**, 2296-2300.